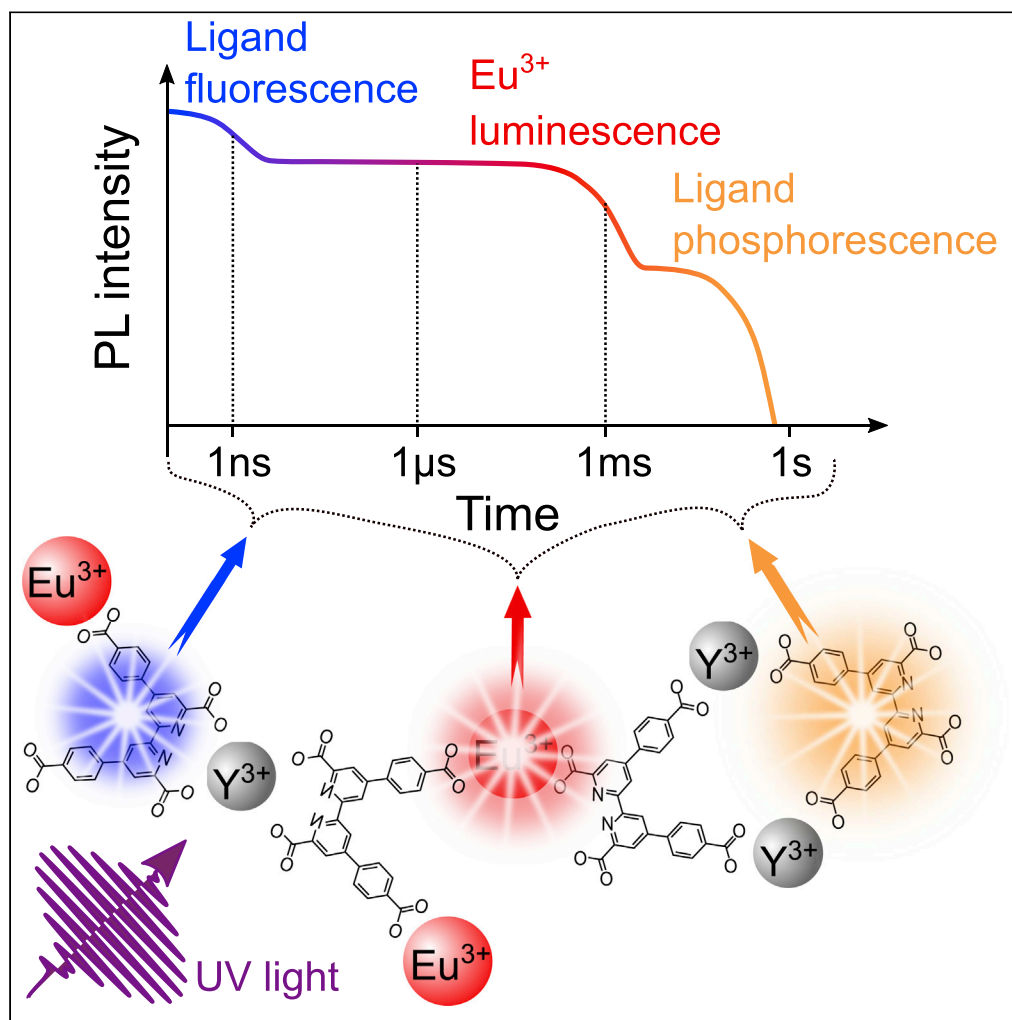**Article**

Rare-earth coordination polymers with multimodal luminescence on the nano-, micro-, and milli-second time scales

Marius Jakoby, Carolin Beil, Pariya Nazari, Bryce S. Richards, Michael Seitz, Andrey Turshatov, Ian A. Howard

michael.seitz@uni-tuebingen.de (M.S.)
andrey.turshatov@kit.edu (A.T.)
ian.howard@kit.edu (I.A.H.)

HIGHLIGHTS

Coordination polymer exhibts nano-, micro-, and milli-second emission bands.

Luminescence observed from ligand singlet and triplet states and lanthanide centers.

Triluminescence is enabled by exciton immobility.

Intersystem crossing is mediated by ligand environment.

Article

Rare-earth coordination polymers with multimodal luminescence on the nano-, micro-, and milli-second time scales

Marius Jakoby,[1] Carolin Beil,[2] Pariya Nazari,[1] Bryce S. Richards,[1,3] Michael Seitz,[2,*] Andrey Turshatov,[1,*] and Ian A. Howard[1,3,4,*]

SUMMARY

We present a coordination polymer based on rare-earth metal centers and carboxylated 4,4′-diphenyl-2,2′-bipyridine ligands. We investigate Y^{3+}, Lu^{3+}, Eu^{3+}, and a statistical mixture of Y^{3+} with Eu^{3+} as metal centers. When Y^{3+} or Lu^{3+} is exclusively present in the coordination polymer, biluminescence from the ligand is observed: violet emission from the singlet state (417 nm, 0.9 ns lifetime) and orange emission from the triplet state (585 nm, 76 ms (Y^{3+}) and 31 ms (Lu^{3+})). When Eu^{3+} is present in a statistical mixture with Y^{3+}, red emission from the Eu^{3+} (611 nm, $\sim$ 500 μs) is observed in addition to the ligand emissions. We demonstrate that this multi-mode emission is enabled by the immobility of singlet and triplet states on the ligand. Eu^{3+} only receives energy from adjacent ligands. Meanwhile, in the broad inhomogeneous distribution of ligand energies, higher energy states favor singlet emission, whereas faster intersystem crossing in the more stabilized ligands enhances their contribution to triplet emission.

INTRODUCTION

In most luminophores, light ceases to be emitted from the material almost immediately once the excitation light is switched off. Materials that show persistent room-temperature phosphorescence (RTP) emit light for a significant period (from seconds to hours) after the excitation source is turned off (Aitasalo et al., 2003) and have attracted great attention for their broad utility in optoelectronics (Zhao et al., 2019), including chemical and temperature sensing (Tang et al., 2013; Chen et al., 2015), bioimaging (Sun et al., 2018; Abdukayum et al., 2013), and anti-counterfeiting (Liu et al., 2018). Classic persistent phosphors include zinc sulfide doped with copper and cobalt (Hoogenstraaten and Klasens 1953; Shionoya et al. 2006), while a breakthrough was achieved by Matsuzawa et al. in 1996 by codoping the green-emitting phosphor $SrAl_2O_4:Eu^{2+}$ with dysprosium, which led to bright persistent luminescence for several hours (Matsuzawa et al., 1996). The afterglow of these rare-earth-doped inorganic crystals is based on the thermal repopulation of the emissive sites from charge-trapping sites inside the crystal lattice (Matsuzawa et al., 1996; Bierwagen et al., 2020).

Another key result in the story of persistent phosphors was the 2006 development of the first organic compound to exhibit persistent luminescence at room temperature (Zhang et al., 2007). In organic materials, the persistent emission is based on a spin-forbidden transition from the triplet excited state to the singlet ground state of the molecule. For this emission, to be efficient the triplet state must be protected from oxygen and from relaxation through non-radiative pathways (vibrations). Beyond encapsulation of the materials, it has been shown that oxygen quenching can be suppressed by stabilizing the triplet state, for example, via H-aggregation (An et al., 2015) or $\pi - \pi$ stacking (J. Yang et al., 2018). Furthermore, incorporation of luminophores as ligands in metal-organic frameworks can stiffen the ligands, suppressing vibrational modes and associated non-radiative relaxation pathways, allowing RTP to be observed in a variety of organic luminophores (Yang and Yan, 2016). A second approach to achieving persistent emission in organic materials uses a blend of electron-donating and electron-accepting materials (Kabe and Adachi 2017). These separate the charge carriers held in the excited state created after photon absorption, with emission then being observed from the subsequent non-geminate recombination at timescales ≫ s (Kabe and

[1]Institute of Microstructure Technology, Karlsruhe Institute of Technology, Hermann-von-Helmholtz-Platz 1, 76344 Eggenstein-Leopoldshafen, Germany

[2]Institute of Inorganic Chemistry, University of Tübingen, Auf der Morgenstelle 18, 72076 Tübingen, Germany

[3]Light Technology Institute, Karlsruhe Institute of Technology, Engesserstrasse 13, 76131 Karlsruhe, Germany

[4]Lead contact

*Correspondence: michael.seitz@uni-tuebingen.de (M.S.), andrey.turshatov@kit.edu (A.T.), ian.howard@kit.edu (I.A.H.)

https://doi.org/10.1016/j.isci.2021.102207

Adachi 2017). This second approach is somewhat equivalent to the charge carrier trapping and release/recombination in the organic materials.

Some materials can combine persistent luminescence with the more standard prompt luminescence (combine phosphorescence and fluorescence) and are referred to as biluminescent (Reineke et al., 2013). Materials exhibiting biluminescence provide access to novel applications and have been used to create re-writable luminescent images (Gmelch et al., 2019), organic light-emitting diodes with afterglow (Kabe et al., 2016), and anti-counterfeiting codes (Yang et al., 2020).

Herein, we present a coordination polymer based on rare-earth metal centers and carboxylated 4,4'-diphenyl-2,2'-bipyridine (CDB) ligands. The metal centers are chosen to be either trivalent yttrium, lutetium, and europium or a statistical mixture of Y^{3+} and Eu^{3+}. In the case that non-optically active Y^{3+} or Lu^{3+} are exclusively present in the coordination polymer, only singlet and triplet emissions from the organic linker are observed, with the former on the nanosecond timescale and the latter on the milli-second timescale (similar to literature-known biluminescent materials). By introducing a statistical mixture of Eu^{3+} and Y^{3+} into the coordination polymer, in addition to retaining the two aforementioned luminescence mechanisms, a third mechanism for emission is added, namely, the microsecond emission of the Eu^{3+} center. This unique triluminescent compound exhibits three luminescent decay mechanisms with lifetimes on the nano-, micro-, and milli-second timescale, respectively. We note that recently also a triluminescent material was demonstrated by Gangwar et al. by admixing an upconverting Yb^{3+}, Er^{3+}-based phosphor (green emission), a down-converting Eu^{3+}-based phosphor (red emission), as well as a downshifting zinc oxide phosphor (green emission) (Gangwar et al. 2018). However, due to the spectrally separated absorption bands of the three mixed emitters, this material requires a distinct excitation wavelength for each emission spectrum, and also, no time-resolved photoluminescence (TRPL) measurements were presented (Gangwar et al. 2018), which clearly delimits it from the triluminescent material presented here.

RESULTS AND DISCUSSION

Biluminescent coordination polymers

In order to observe both singlet and triplet emissions from the organic ligands in the coordination polymer, two requirements should be satisfied. Firstly, enough of the singlets (created after photo-excitation) should intersystem cross to the triplet state such that there is an appreciable population of the triplet state for emission to be observable. Secondly, the rate of the radiative transition from the excited triplet state to singlet ground state should be comparable to the non-radiative decay channel such that the triplet emission is observable.

In order to satisfy the first requirement, we choose the CDB as the ligand for the coordination polymer. The combination of the benzoate/phenylcarboxylate together with the bipyridine structural motive leads to a reasonable coupling between the singlet and triplet state manifold since the lone pair electrons promote $n \rightarrow \pi^*$ transitions (Xu et al., 2016; Li and Li 2017). Furthermore, the close proximity to the rare-earth centers will significantly assist in the intersystem crossing (ISC), as well as in allowing the radiative transfer from the first excited triplet to the ground state. Support for this will be presented later in terms of the slightly different lifetimes of the triplet emission when the metal center is changed from Y^{3+} to Lu^{3+}.

Figure 1A shows the chemical structure of the ligand, alongside a schematic showing the average stoichiometry of a repeat unit in the CDB coordination polymer's (amorphous) structure. The ligand to metal center ratio is 3:2 and the ligand to triethylammonium is 2:1 (determined by elemental analysis and NMR, see Figures S10 and S11 and supplemental information section ii, transparent methods: synthesis). As discussed in Figure S1, we hypothesize that a densely cross-linked 3D structure is created: the three binding sites per ligand allowing ligands to interact with metal centers in a variety of ways creating a wide variety of local environments for a ligand and the suppression of the ingress of oxygen into the material (Klinger et al., 2009; Gordon and Ravve 1980) (consistent with the photophysical data presented following). We also note that the geometry of two ligands that are bound via their central bonding site to a metal center should exhibit a dihedral angle between the two planar ligand fragments of about 89°, as determined for an analogous linker lacking the two carboxylic groups at the terminal positions (Kruck et al., 2019).

In order to satisfy the second requirement, the similarity of radiative and non-radiative rates from the triplet state, we postulate that as in metal-organic frameworks (Wei et al., 2014; Ma et al., 2017) and covalent
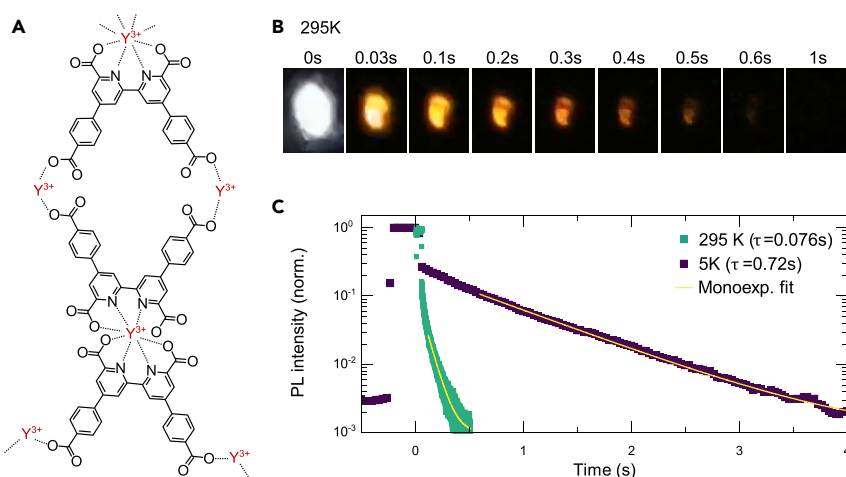
Figure 1. Structure and room-temperature phosphorescence of the Y^{3+}-based coordination polymer
(A) Biluminescent CDB coordination polymer based on Y^{3+} metal centers, illustrating the ligands and amorphous structure of the CDB coordination polymer.
(B) Illustration of biluminescence from frames of a video recording the PL emission at 295 K.
(C) Time-resolved PL emission intensity at 295 K and 5 K.

organic frameworks (Li et al., 2018), the rigidification of the ligands upon incorporation into the extended covalent framework will suppress the non-radiative vibrational relaxations of the triplet excited state to such an extent that RTP becomes observable. Also, as mentioned above, the heavy-atom effect of the neighboring metal centers should assist in increasing the radiative coupling between the excited triplet state and the singlet ground state.

Confirming our expectations, biluminescence is indeed observed from the Y^{3+}-based CDB coordination polymer. This is visually introduced in Figure 1B, wherein both the prompt nanosecond luminescence and delayed phosphorescence from the sample after excitation are visible (excitation was with a quasi-continuous wave modulated diode laser at 405 nm, 0.1 W cm^{-2}, 0.2 Hz, and 10% duty cycle, and the prompt emission saturates the camera so that the delayed luminescence is easily seen). The extracted video frames (captured with a smartphone) demonstrate that the RTP is bright enough to see by eye.

Figure 1C then shows the TRPL kinetics of the samples at room temperature and 5 K measured by multi-channel scaling (see the experimental section, time resolution: 0.128 μs) and a mobile phone camera (30 fps), respectively. The nanosecond decay of the singlet state is registered as the sudden decay after the excitation light is switched off during which the intensity drops to roughly 0.3 of its initial value for the room temperature experiment. This fraction is slightly higher for the low-temperature experiment, as the yield of triplet states created by ISC will slightly increase at low temperature since the competitive rate of non-radiative recombination of the singlet is suppressed. Importantly, the lifetime of the triplet emission is 76 ms and 720 ms at room temperature and 5 K, respectively, determined by the monoexponential fits shown in Figure 1C. Making the standard assumption that the quantum yield of emission from the triplet state is 100% at 5 K, the order of magnitude reduction in the lifetime from 5 K to room temperature suggests that the photoluminescence quantum yield (PLQY) of a triplet state (once it is formed) is around 10% at room temperature. However, in order to get the total PLQY of the triplet state per absorbed photon at room temperature, this 10% must be multiplied by the probability that one of the initially created singlet states undergoes ISC to form the triplet.

Despite the triplet nature of the delayed emission, its intensity and lifetime are not sensitive to oxygen. To test this, we placed a powder of the Y^{3+}-based CDB coordination polymer that was stored in ambient air for several weeks into a vacuum chamber. We first measured the photoluminescence (PL) transient before starting the vacuum pump and remeasured after the sample was exposed to dynamic vacuum with pressures below 1×10^{-5} mbar for 1 hr and 24 hr (see Figure S2). No change in lifetime between the sample measured under vacuum and the sample stored in air for long periods was observed. This is consistent
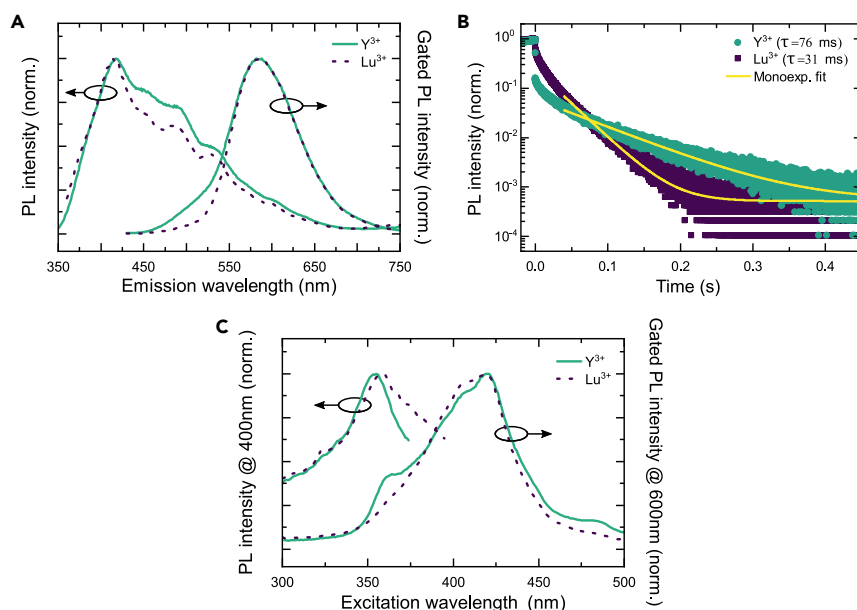
Figure 2. Biluminescence of the Y³⁺-based and Lu³⁺-based coordination polymers

(A) Steady-state PL and gated PL (0.1 ms to 250 ms) spectra under 350 nm and 420 nm excitation, respectively.

(B) PL kinetics collecting photons at 600 nm.

(C) Steady-state and gated (0.1 ms to 250 ms) excitation spectra collecting photons at 410 nm and 600 nm, respectively.

with results on metal-organic frameworks (Yang and Yan, 2016) and densely packed organic crystals (J. Yang et al., 2018), which exhibit bright RTP in air.

In order to gain a deeper understanding of the biluminescence of these samples, we study the gated PL and lifetime of CDB coordination polymers based on both Y³⁺ and Lu³⁺ as shown in Figure 2. In Figure 2A, we present the time-integrated PL (steady-state PL) and compare it to the gated PL collected from 0.1 ms to 250 ms after excitation. The fluorescence spectra of both CDB coordination polymers peak at 417 nm, and further peaks are visible on the low energy side as discussed later. In contrast, the phosphorescence spectra are featureless and centered around 585 nm. The energy difference between the singlet and triplet energy is therefore around 0.85 eV, reasonable for an organic chromophore.

The TRPL results measured with multi-channel scaling for the Y³⁺- and Lu³⁺-based CDB coordination polymers are shown in Figure 2B. Interestingly, the triplet lifetime depends on the metal center, with the longest-lived tail of the Lu³⁺-based material having a lifetime of 31 ms, whereas the lifetime of the Y³⁺-based material is 76 ms as previously determined. This difference in triplet lifetime is evidence that the interaction of (at least a subset) organic ligands with the particular metal center in the CDB coordination network affects their spin dynamics. The singlet lifetime of the lower energy emissive states (measured by streak camera, Figure S3), on the other hand, remains constant at 0.8 ns. We note that the distribution of ligand environments for triplet states would lead to the decay not being purely monoexponential. The fact that triplet decay is well expressed by a single exponential after 0.05 s is consistent with the other photophysical evidence that triplets are created preferentially at a subset of lower energy sites that are relatively similar to one another.

Finally, Figure 2C depicts the excitation spectra of the two samples for the fluorescence and phosphorescence emission spectrum. Firstly, the fluorescence PL intensity at 410 nm is monitored. This PL reaches a maximum intensity for an excitation wavelength of 350 nm. Secondly, the phosphorescence PL intensity at 600 nm in a gated measurement is measured as a function of the excitation wavelength. In this case, the peak emission is observed when the excitation wavelength is 420 nm (well within the emission of the singlet). The two separate absorption bands that lead to the singlet and triplet emission suggest that separate (absorbing) states contribute differently to the prompt emission (measured at 410 nm) and the delayed emission.

We hypothesize that there is a significant energetic disorder in the amorphous CDB coordination polymers, due to differing numbers and distances of nearest metal centers to individual ligands. This suggestion of a large inhomogeneous energetic disorder is strongly supported by the observation that the steady-state emission spectrum shifts strongly as the excitation wavelength is scanned (Figure S4). This suggests that many subsets of the ligand population exist, with absorption and emission spectra that are stabilized by varying amounts depending on their local environment. The low energy features on the very broad singlet PL band observed in Figure 2A are most likely (at least partially) due to this inhomogeneous broadening. The triplet emission is strongest from the most stabilized states, potentially because ISC is the fastest in these due to their stronger interaction with metal centers. This interpretation is supported by the anomalous decrease in the PL lifetime for longer emission wavelengths (see Figure S8). The atypical decrease in the lifetime of the lower energy states with respect to the higher energy states confirms that singlet migration is not efficient in this material (otherwise the lifetime of the lower energy states would be increased by migration of energy from the higher energy states). Furthermore, the shorter lifetime of the lower energy states is consistent with increased ISC due to the stronger interaction with the metal centers.

We note that this situation differs slightly from the effects of crystallization exploited to engineer RTP from purely organic luminogens. For these organic compounds, the relative stacking of molecules is of utmost importance for enabling efficient reverse intersystem crossing (RISC) (Li and Li 2017; Hamzehpoor and Perepichka 2020). For these purely organic crystals, the increase of the singlet lifetime due to a decrease in the radiative rate caused by H-aggregation in the crystal form enhances the fraction of singlets that can undergo ISC and ultimately lead to RTP. However, if H-aggregation were to play a major role in triplet generation in our material, we would expect the lifetime of the lower energy states (those from which triplets are most efficiently created) to be longer than the higher energy states. Given the contrary is true that the lower energy states are shorter lived, we conclude that the enhanced RTP in our materials is not related to H-aggregation in the coordination polymer. However, similar to the organic crystals and previous work on metal-organic frameworks, the suppression of non-radiative relaxation due to increased rigidity of the linkers in the framework will be favorable for RTP (Li and Li 2017; Zhao et al., 2019).

Returning to the consideration of our material, the dependence of the singlet versus triplet yield on the site energy means that the ratio of the prompt to delayed emission can be varied by selecting the excitation wavelength. To gain an indicative value for the efficiency of the emission, we measure the PLQY of the total emission from the ligand after excitation at 405 nm. The PLQY is low at only 1% and, in conjunction with reasonable lifetimes, suggests that there may be a significant portion of static quenching by quenching sites. Those quenching sites for the ligands' luminescence might stem from the energetic disorder in the coordination polymer, and only a small subset of the ligands that are not adjacent to such quenching sites participate in emission.

Triluminescent CDB coordination polymers

As demonstrated in the previous section, CDB coordination polymers utilizing Y^{3+} and Lu^{3+} are biluminescent materials with ligand-based emission on the ns timescale (fluorescence) and ms timescale (phosphorescence). In the following, we investigate the possibility of adding a third decay component in the μs range by codoping the Y^{3+}-based CDB coordination polymer with optically active Eu^{3+}.

In Figure 3 steady-state PL spectra as well as PL kinetics of the Y^{3+}-based CDB coordination network with different amount of Eu^{3+} doping are illustrated (0–50% of the Y^{3+} replaced by Eu^{3+}). For the PL spectra (see Figure 2A), the sample is excited at 350 nm. The distinct red transitions of Eu^{3+} are clearly visible in all Eu^{3+}-doped samples (with the most prominent transition at 610 nm). The organic ligand can act as a sensitizer of the Eu^{3+} emission. The singlet energy from a ligand can be transferred to a Eu^{3+} acceptor. The distance a singlet exciton can travel, hopping between ligands, can be estimated by a Stern-Volmer analysis of the quenching of the ligand singlet PL as a function of the Eu^{3+} doping concentration. Such an analysis (see section sii, transparent methods: Stern-Volmer analysis for further details and experimental data) reveals that the singlet state moves at maximum around 1 ligand length, suggesting singlet hopping between ligands does not occur. This suggests that only singlet excitons created in the direct vicinity of Eu^{3+} are quenched. Analysis of the PL lifetime of the singlet exciton as a function of Eu^{3+} confirms this. Although the magnitude of the singlet PL is decreased by the addition of Eu^{3+}, the lifetime of the PL remains constant (see Figure S7). Thus, singlet excitons created outside the immediate vicinity of a Eu^{3+} ion are not affected by its presence. They cannot migrate between ligands and therefore are not quenched.
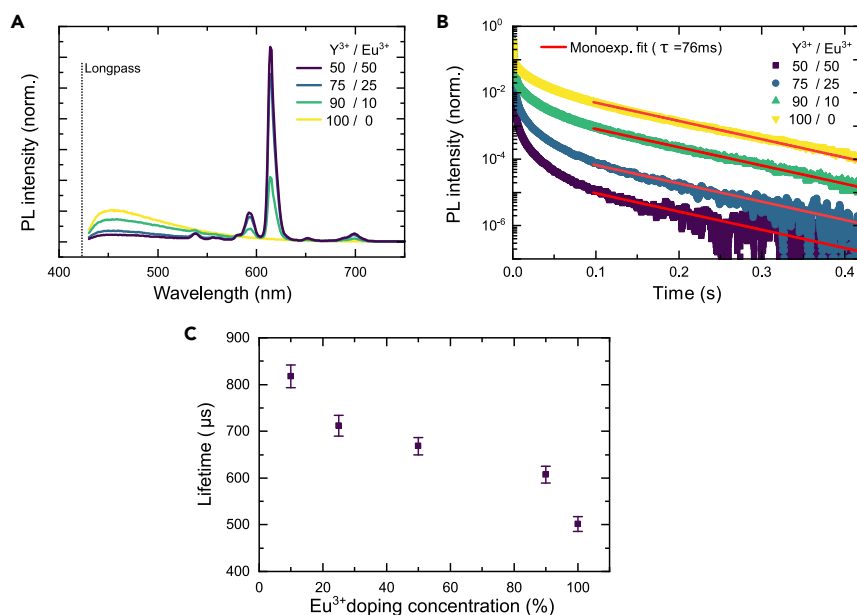
Figure 3. Triluminescence of the Y^{3+}-based coordination polymer by doping with Eu^{3+}

(A) Steady-state PL spectra as a function of the Eu^{3+} concentration. The excitation is at 350 nm, and each spectrum is normalized to the area under the curve. Fluorescence and phosphorescence from the ligand are observable alongside the characteristic longer wavelength Eu^{3+} emission.

(B) Excitation at 405 nm and collection at 630 nm.

(C) Averaged PL lifetimes of the Eu^{3+} emission at 610 nm extracted from biexponential fits to the PL kinetics shown in Figure S6. The error bars are based on the standard deviation of five measurements at different sample positions.

Figure 3B demonstrates that the triplet quenching is also only static. Although the amount of the delayed emission is reduced, its lifetime is not. Thus, not all of the excited states transfer to the Eu^{3+} complex but only those that are created in the direct vicinity of a Eu^{3+} metal center. This means that both the singlet and triplet emissions (from ligands near only Y^{3+} metal centers) remain observable at the same time as the new 610 nm emission from the Eu^{3+} center.

Figure 3C shows the Eu^{3+} emission lifetime as a function of the Eu^{3+} doping concentration in the material. The lifetime decreases from 820 μs at low Eu^{3+} concentrations to 500 μs at higher concentrations. This is consistent with the following: (i) concentration quenching due to killer sites and (ii) our previous discussion of disorder in these amorphous materials, with certain Eu^{3+} sites likely having fast non-radiative decay channels due to their local environment (potentially dangling bonds). Once the Eu^{3+} concentration becomes high enough that energy transfer between Eu^{3+} ions to these inefficient sites becomes possible, then the Eu^{3+} lifetime (and emission efficiency) will start to decrease.

The PLQY of only the Eu^{3+} emission as a function of Eu^{3+} concentration after exciting the ligand at either 300 nm or 405 nm is shown in Figure S5. The PLQY increases with increasing Eu^{3+} concentration, as a greater fraction of the excited ligands can transfer their energy to a Eu^{3+} center. Only at the highest Eu^{3+} concentration does the PLQY again fall, due to the aforementioned reduction of lifetime due to killer sites negating the effect of increased energy transfer from the ligands. The PLQY of the Eu^{3+} emission is in the range of 2%–15%, depending on the excitation wavelength and Eu^{3+} concentration. This is superior to the ligand PLQY alone, suggesting that energy transfer from linkers to adjacent Eu^{3+} ions is fast, and can outcompete the transfer to an adjacent killer site.

Conclusions

We have developed a sequence of CDB coordination polymers based on Y^{3+}, Lu^{3+}, and a statistical mixture of Y^{3+} and Eu^{3+} metal centers. We demonstrated that biluminescence from the ligand can be achieved in the coordination polymers based on Y^{3+} and Lu^{3+}. Herein, a singlet emission with a lifetime

of 0.9 ns and peak wavelength of 417 nm is observed, alongside a triplet emission whose peak wavelength is shifted to 585 nm and has a room temperature lifetime of 76 ms for the Y^{3+}-utilizing material and 31 ms for the Lu^{3+} case. At 5 K, the triplet lifetime in the Y^{3+} material is extended to 720 ms. Furthermore, we show that by utilizing a statistical mixture of Y^{3+} and Eu^{3+} for the metal centers, the two above mentioned modes of luminescence can be retained and a third luminescence mode added, namely, the narrow-band emission from the Eu^{3+} ion centered at 610 nm. This has a lifetime varying between 700 ms and 500 ms, with the lifetime decreasing to the latter value as the fraction of the metal centers occupied by Eu^{3+} reaches 50%.

The physical mechanisms underlying the ability of this material to sustain these 3 modes of fluorescence are (1) inhomogeneous disorder in the ligand energies and (2) immobility of ligand singlet and triplet states. The immobility of the singlet and triplet states on the ligand means that the Eu^{3+} metal centers only receive energy from ligand singlet states in their direct vicinity. Singlet and triplet states created further away from the Eu^{3+} center are not affected at all; their lifetime and emission are unaffected by the presence of the Eu^{3+}. The lower energy ligand states that are more stabilized by interaction with Y^{3+} or Lu^{3+} metal centers exhibit faster ISC and therefore contribute more to the triplet emission from the material. Singlet emission is preferential for the higher energy ligand states, which, again due to the lack of singlet motion in these materials, cannot transfer their energy to shorter-lived lower-energy ligand states.

Thus, we demonstrate that coordination polymers based on rare-earth metal centers and appropriately chosen organic linkers allow novel materials to be made that display three unique luminescent emissions with lifetimes on the nano-, micro-, and milli-second timescale, respectively. While the biluminescent material could be used for smartphone-based temperature measurement due to its long PL lifetime, the unique signature of the PL kinetics of the triluminescent material is a promising feature for its application as an advanced anti-counterfeiting label.

Limitations of the study

This initial study demonstrates the feasibility of generating biluminescent and triluminescent materials based on coordination polymers with rare-earth metal centers. This first generation of material is amorphous, leading to a high degree of energetic disorder caused by the varying local environments for individual ligands (and rare-earth ions). Designing covalent organic frameworks with defined structures and similar ligands would be an avenue to study the photophysics of the linker and lanthanide emission with better defined energy levels. This could be an important route to increase the currently low PLQY of only 1% from the ligand emission.

The significant change of the triplet emission's lifetime from room temperature to 5 K indicates that there is still a high potential (factor of 10) for increasing the brightness of the persistent luminescence part of the emission of the coordination polymer at room temperature by suppressing non-radiative decay channels. Here, a possible direction would be to further rigidify the organic ligand by exchanging the bonds between dipyridine and phenyl units in a fluorene-type manner or to explore crystal engineering strategies to further reduce the vibrational freedom of the linkers (Yang et al., 2018).

Applications were not explored in this first proof-of-principle study. However, based on further development of adjustable disparate lifetimes and intensity ratios in a single material, potential applications as a photonic dye for luminescence imaging, sensing, and anti-counterfeiting could be considered. In order to pave the way for such applications, development of nanoparticles of these triluminescent materials would be a promising approach.

Resource availability

Lead contact

Further information and requests for resources should be directed to and will be fulfilled by the lead contact, Ian Howard (ian.howard@kit.edu).

Material availability

This study did not generate new unique reagents.

METHODS

All methods can be found in the accompanying transparent methods supplemental file.

SUPPLEMENTAL INFORMATION

Supplemental information can be found online at https://doi.org/10.1016/j.isci.2021.102207.

AUTHOR CONTRIBUTIONS

Conceptualization, M.J., I.A.H., A.T., and M.S.; Synthesis, C.B., and M.S.; Methodology, M.J. and C.B.,; Investigation, M.J. and P.N.; Writing—Original Draft, M.J. and I.A.H.; Writing—Review & Editing, all authors; Funding Acquisition, B.S.R., I.A.H. A.T. and M.S.

DECLARATION OF INTERESTS

Subsequently to this work P.N. became affiliated with Innovation Lab GmbH, Speyerer Strasse 4, 69115 Heidelberg, Germany.

REFERENCES

Abdukayum, A., Chen, J.-T., Zhao, Q., and Yan, X.-P. (2013). Functional near infrared-emitting Cr3+/Pr3+ Co-doped zinc gallogermanate per sistent luminescent nanoparticles with superlong afterglow for in vivo targeted bioimaging. J. Am. Chem. Soc. 135, 14125–14133.

Aitasalo, T., Dereń, P., Hölsä, J., Jungner, H., Krupa, J.-C., Lastusaari, M., Legendziewicz, J., Niittykoski, J., and Strek, W. (2003). Persistent luminescence phenomena in materials doped with rare earth ions. J. Solid State. Chem. 171, 114–122, Proceedings from the 23rd Rare Earth Research Conference UC Davis Campus, July 13-16, 2002.

An, Z., Zheng, C., Tao, Y., Chen, R., Shi, H., Chen, T., Wang, Z., Li, H., Deng, R., Liu, X., and Huang, W. (2015). Stabilizing triplet excited states for ultralong organic phosphorescence. Nat. Mater. 14, 685–690.

Bierwagen, J., Delgado, T., Jiranek, G., Yoon, S., Gartmann, N., Walfort, B., Pollnau, M., and Hagemann, H. (2020). Probing traps in the persistent phosphor SrAl2O4:Eu2+,Dy3+,B3+ - a wavelength, temperature and sample dependent thermoluminescence investigation. J. Lumin. 222, 117113.

Chen, D., Wan, Z., Zhou, Y., Zhou, X., Yu, Y., Zhong, J., Ding, M., and Ji, Z. (2015). Dual-phase glass ceramic: structure, dual-modal luminescence, and temperature sensing behaviors. ACS Appl. Mater. Inter. 7, 19484–19493.

Gangwar, A.K., Nagpal, K., and Gupta, B.K. (2018). Triluminescent functional composite pigment for non-replicable security codes to combat counterfeiting. ChemistrySelect 3, 9627–9633.

Gmelch, M., Thomas, H., Fries, F., and Reineke, S. (2019). Programmable transparent organic luminescent tags. Sci. Adv. 5, 2.

Gordon, G.A., and Ravve, A. (1980). Oxygen transmission through highly crosslinked polymers. Polym. Eng. Sci. 20, 70–77.

Hamzehpoor, E., and Perepichka, D.F. (2020). Crystal engineering of room temperature phosphorescence in organic solids. Angew. Chem. Int. Ed. 59, 9977–9981.

Hoogenstraaten, W., and Klasens, H.A. (1953). Some Properties of Zinc Sulfide Activated with Copper and Cobalt. J. Electrochem. Soc 100, 366.

Kabe, R., and Adachi, C. (2017). Organic long persistent luminescence. Nature 550, 384–387.

Kabe, R., Notsuka, N., Yoshida, K., and Adachi, C. (2016). Afterglow organic light-emitting diode. Adv. Mater. 28, 655–660.

Klinger, M., Tolbod, L.P., Gothelf, K.V., and Ogilby, P.R. (2009). Effect of polymer cross-links on oxygen diffusion in glassy PMMA films. ACS Appl. Mater. Inter. 1, 661–667.

Kruck, C., Nazari, P., Dee, C., Richards, B.S., Turshatov, A., and Seitz, M. (2019). Efficient ytterbium near-infrared luminophore based on a nondeuterated ligand. Norg. Chem. 58, 6959–6965.

Li, Q., and Li, Z. (2017). The strong light-emission materials in the aggregated state: what happens from a single molecule to the collective group. Adv. Sci. 4, 1600484.

Li, Q., Tang, Y., Hu, W., and Li, Z. (2018). Fluorescence of nonaromatic organic systems and room temperature phosphorescence of organic luminogens: the intrinsic principle and recent progress. Small *14*, 1801560.

Liu, J., Zhuang, Y., Wang, L., Zhou, T., Hirosaki, N., and Xie, R.-J. (2018). Achieving multicolor long-lived luminescence in dye-encapsulated metal–organic frameworks and its application to anticounterfeiting stamps. ACS Appl. Mater. Inter. *10*, 1802–1809.

Ma, L., Feng, X., Wang, S., and andWang, B. (2017). Recent advances in AIEgenbased luminescent metal–organic frameworks and covalent organic frameworks. Mater. Chem. Front. *1*, 2474–2486.

Matsuzawa, T., Aoki, Y., Takeuchi, N., and Murayama, Y. (1996). A new long phosphorescent phosphor with high brightness, SrAl2O4 : Eu2 ,Dy3. J. Electrochem. Soc. *143*, 2670–2673.

Reineke, S., Seidler, N., Yost, S.R., Prins, F., Tisdale, W.A., and Baldo, M.A. (2013). Highly efficient, dual state emission from an organic semiconductor. Appl. Phys. Lett. *103*, 093302.

Shionoya, S., Yen, W.M., and Yamamoto, H. (2006). Phosphor Handbook, Second Edition (CRC Press).

Sun, S.-K., Wang, H.-F., and Yan, X.-P. (2018). Engineering persistent luminescence nanoparticles for biological applications: from biosensing/bioimaging to theranostics. Acc. Chem. Res. *51*, 1131–1143.

Tang, Y., Song, H., Su, Y., and Lv, Y. (2013). Turn-on persistent luminescence probe based on graphitic carbon nitride for imaging detection of biothiols in biological fluids. Anal. Chem. *85*, 11876–11884.

Wei, Z., Gu, Z.-Y., Arvapally, R.K., Chen, Y.-P., McDougald, R.N., Ivy, J.F., Yakovenko, A.A., Feng, D., Omary, M.A., and Zhou, H.-C. (2014). Rigidifying fluorescent linkers by metal–organic framework formation for fluorescence blue shift and quantum yield enhancement. J. Am. Chem. Soc. *136*, 8269–8276.

Xu, S., Chen, R., Zheng, C., and Huang, W. (2016). Excited state modulation for organic afterglow: materials and applications. Adv. Mater. *28*, 9920–9940.

Yang, J., Zhen, X., Wang, B., Gao, X., Ren, Z., Wang, J., Xie, Y., Li, J., Peng, Q., Pu, K., and Li, Z. (2018). The inuence of the molecular packing on the room temperature phosphorescence of purely organic luminogens. Nat. Commun. *9*, 840.

Yang, S., Zhou, B., Huang, Q., Wang, S., Zhen, H., Yan, D., Lin, Z., and Ling, Q. (2020). Highly efficient organic afterglow from a 2D layered lead-free metal halide in both crystals and thin films under an air atmosphere. ACS Appl. Mater. Inter. *12*, 1419–1426.

Yang, X., and Yan, D. (2016). Strongly enhanced long-lived persistent room temperature phosphorescence based on the formation of metal–organic hybrids. Adv. Opt. Mater. *4*, 897–905.

Zhang, G., Chen, J., Payne, S.J., Kooi, S.E., Demas, J.N., and Fraser, C.L. (2007). Multi-emissive diuoroboron dibenzoylmethane polylactide exhibiting intense fluorescence and oxygen-sensitive room-temperature phosphorescence. J. Am. Chem. Soc. *129*, 8942–8943.

Zhao, Y., Yang, X.-G., Lu, X.-M., Yang, C.-D., Fan, N.-N., Yang, Z.-T., Wang, L.-Y., and Ma, L.-F. (2019). Zn6 cluster based metal–organic framework with enhanced room-temperature phosphorescence and optoelectronic performances. Inorg. Chem. *58*, 6215–6221.

Supplemental information

Rare-earth coordination polymers with multimodal

luminescence on the nano-, micro-, and milli-second

time scales

Marius Jakoby, Carolin Beil, Pariya Nazari, Bryce S. Richards, Michael Seitz, Andrey Turshatov, and Ian A. Howard

Supplemental Information

Rare-earth coordination polymers with multimodal luminescence on the nano-, micro-, and milli-second time scales

Marius Jakoby[a], Carolin Beil[b], Pariya Nazari[a], Bryce S. Richards[a,c], Michael Seitz[b,*], Andrey Turshatov[a,*], Ian A. Howard[a,c,1,*]

[a]*Institute of Microstructure Technology, Karlsruhe Institute of Technology, Hermann-von-Helmholtz-Platz 1, D-76344Eggenstein-Leopoldshafen, Germany*
[b]*Institute of Inorganic Chemistry, University of Tübingen, Auf der Morgenstelle 18, 72076 Tübingen, Germany*
[c]*Light Technology Institute, Karlsruhe Institute of Technology, Engesserstrasse 13, D-76131 Karlsruhe, Germany*

SI. Additional Figures

[*]Email adresses: ian.howard@kit.edu, andrey.turshatov@kit.edu, michael.seitzd@uni-tuebingen.de
[1]Lead contact
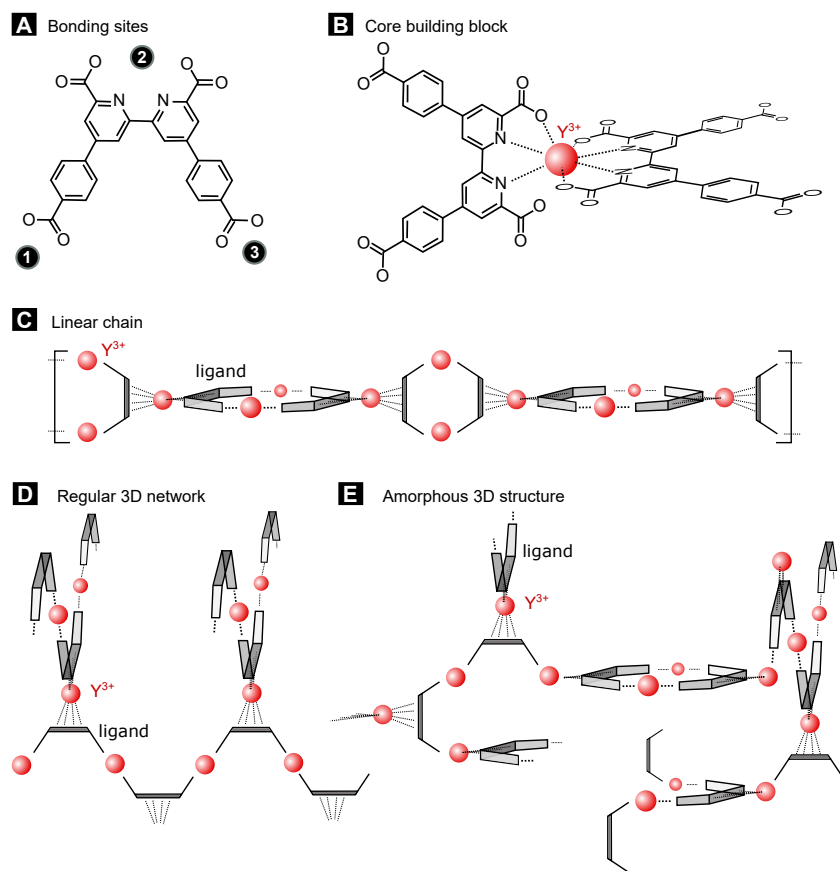
Figure S1: (A) Illustration of the three bonding sties of the tritopic linker. (B) Schematic illustration of the the core building block, a D2d-symmetric rare-earth unit (coordination number 8 with two different bipyridine-dicarboxylate ligand units bound). The orientation of the two ligands is based on semiempirical calculations of the equilibrium geometry of a structurally similar linker, which differs only in the absence of carboxyl groups at binding sites one and two. These calculations suggest an angle between the two planar ligand fragments of about 89° (Kruck et al. 2019). (C-E) Possible structures that would be in accordance with the elemental analysis and solid-state NMR (see section III Synthesis). These data indicate a ratio of 3 metal centers to 2 ligands, and also a ratio of 1 $HNEt_3^+$ molecule to 2 ligands. (C) Schematic illustration of a linear chain solely based on the core building block and (D) of a regular 3D structure. (E) Illustration of an amorphous structure as a result of many defects within the regular 3D structure. Here, the densely-crosslinked amorphous 3D structure leads to many different environments of ligands (i.e. number of bound metal sites and nature of the binding to them) are possible and are consistent with the photophysical findings that a range of different non-communicating ligand states exist in the material. Related to Figure 1A.
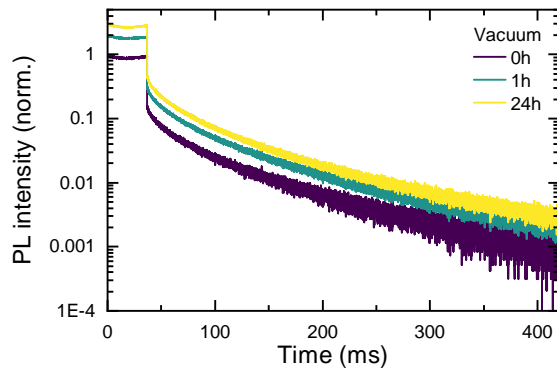
Figure S2: Time-resolved photoluminescence decay of the Y-based 3D CDB coordination polymer for different times in a dynamic vacuum chamber at pressures below 1×10^{-5} mbar. Please note that an offset between the kinetics was introduced to ensure visibility of all three kinetics. This figure demonstrates that the phosphorescence of the ligand is not sensitive to ambient oxygen concentrations. Related to Figure 1.
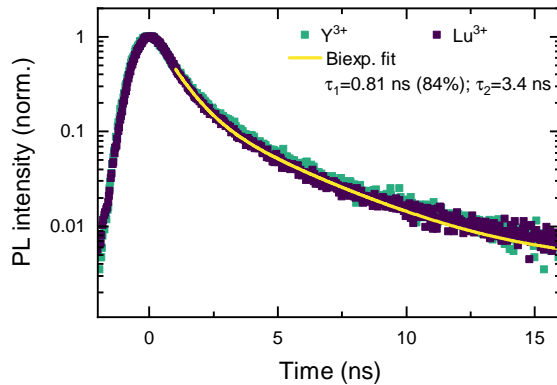

Figure S3: Ligand fluorescence kinetics accompanied by a biexponential fit. The samples were excited at 355 nm and emitted photons in the spectral range of 400 nm to 500 nm integrated for the plotted PL transients. Related to Figure 2B.
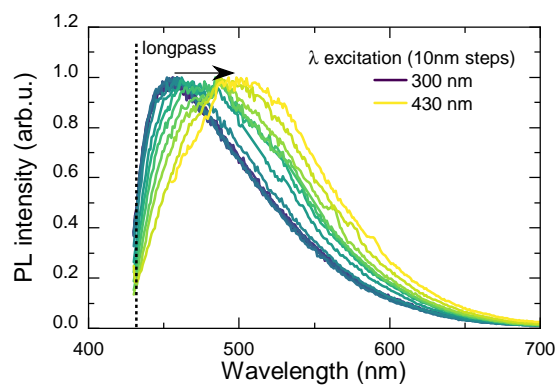
Figure S4: Ligand emission spectra for various excitation wavelengths ranging from 300 nm to 430 nm. Related to Figure 2A.
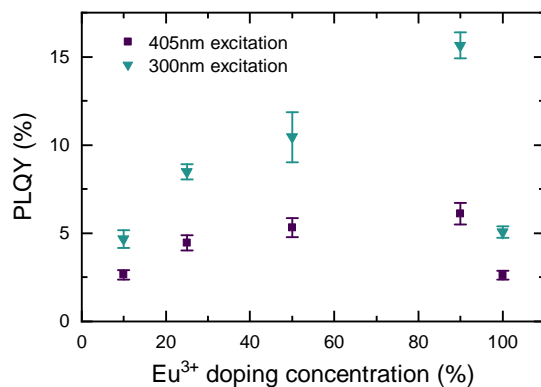
Figure S5: PLQY of the Eu^{3+} luminescence as a function of Eu^{3+} doping concentration in the Y^{3+}-based coordination polymer. The (mean) values and error bars were determined from five measurements at different sample positions. Related to Figure 3.
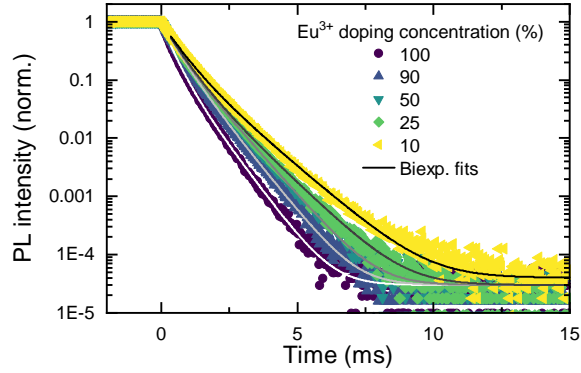
Figure S6: PL kinetics of the Eu^{3+} luminescence at $610\,nm$ as a function of Eu^{3+} doping concentration in the Y^{3+}-based coordination polymer.The fitting parameters are summarized in Table S1. Related to Figure 3.

Eu^{3+} (%)	τ_1 (μs)	A_1	τ_2 (μs)	A_1	τ_{avg} (μs)
100	340	0.65	700	0.25	500
90	420	0.60	750	0.43	610
50	400	0.55	820	0.46	670
25	500	0.69	980	0.28	710
10	540	0.64	1100	0.31	820

Table S1: Extracted parameters from biexponential fits shown in Figure S6. The average lifetime τ_{avg} was determined according to $\tau_{avg} = (A_1\tau_1^2 + A_2\tau_2^2)/(A_1\tau_1 + A_2\tau_2)$. Related to Figure 3.
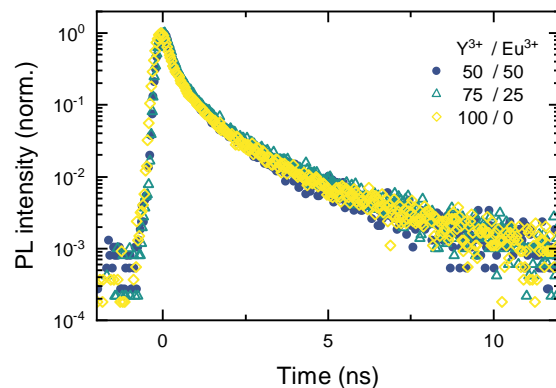
Figure S7: PL kinetics of the excited singlet ligand state of the Y^{3+} -based coordination polymer for different Eu^{3+} doping concentrations. Instead of the Q-switched laser used as the excitation source in all other ns timescale measurements, the third harmonic (343 nm, $90 \, nJ/cm^2$) of a mode-locked ytterbium laser (Light Conversion, Pharos) with a pulse width of 190 fs was employed here to increase the time resolution. Related to Figure 3.
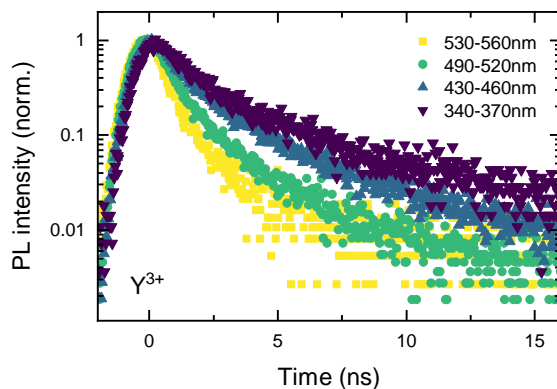

Figure S8: PL kinetics of the excited singlet ligand state of the Y^{3+} -based coordination polymer for different emission wavelengths. The decrease in lifetime with increasing wavelength leads to two conclusions. Firstly, taken in conjunction with the evidence that the triplet emission is more efficiently created by longer wavelength excitation (Figure 2c in the manuscript), this reduced lifetime at longer wavelengths suggests that the intersystem crossing (ISC) rate is increased in the lower energy states. We postulate that stronger interactions with the Y^{3+} metal centers both stabilize these states (red-shifting their singlet emission) in addition to increasing the rate of ISC. Secondly, the shorter lifetime of the lower energy emission supports the findings of poor energy transport in this disordered material. The shorter lifetime of the longer wavelength emission is direct evidence that lower energy sites cannot be populated by the longer-living higher energy sites. Related to Figure 2

6

SII. Transparent Methods

Emission and excitation spectra. Steady-state PL end excitation spectra were collected using a spectrofluorometer (Varian Cary Eclipse) with a built-in xenon flash lamp as excitation source (lamp pulse width at half peak height $\sim 2\,\mu s$, peak power equivalent to $75\,kW$).

Photoluminescence quantum yield. The PLQY measurements were performed according to de Mello *et al.* (Mello, Wittmann, and Friend 1997). Here an integrating sphere (Labsphere CSTM-QE-060-SL, diameter of $15\,cm$) together with a fiber-coupled irradiance calibrated CCD spectrometer (Avantes Inc. AvaSpec-ULS2048x64-TEC) and a $405\,nm$ CW laser source (Roithner LaserTechnik RLT405-10MGS, $10\,mW$) as well as a $300\,nm$ LED (Thorlabs M300L4, $26\,mW$) was employed.

PL transients on the μs and ms time-scale. The time-resolved phosphorescence and Eu^{3+} luminescence kinetics were measured using a multi-channel scaling setup. The sample was excited at $405\,nm$ by a modulated ($0.2\,Hz$ and $10\,\%$ duty cycle) CW laser diode. For the detection, a double monochromator (Bentham DTMS300) and a photomultiplier tube (Hamamatsu R928P) were utilized. The PL kinetics were obtained from the PMT signal using multichannel-scaling electronics (PicoQuant TimeHarp 260 NANO) with a time resolution down to $128\,ns$.

PL transients on the ns time-scale. The time-resolved fluorescence kinetics were measured with a streak camera system. As excitation, the third harmonic of an actively Q-switched laser (Innolas picolo-AOT MOPA) with a wavelength of $355\,nm$, repetition rate of $10\,kHz$, and pulse length of $500\,ps$ was used. The streak camera (Hamamatsu Universal Streak Camera C10910) was used in single-sweep mode to allow for a time-base of $20\,ns$ and a Full width at half maximum (FWHM) of the instrumental-response function of $310\,ps$. The PL kinetics were measured with an excitation fluence of $120\,nJ\,cm^{-2}$.

Temperature-dependent PL kinetic. For the cooling of the sample, a closed-cycle cryostat (Oxford Instruments Optistat Dry TLEX) was used. For the measurement of the phosphorescence kinetic, the camera of a mobile phone (Huawei P30) was utilized.

Stern-Volmer Analysis

A Stern-Volmer (SV) analysis was performed based on the quenching of the photoluminescence quantum yield (PLQY) of the ligand by Eu^{3+}. Here, only the quenching of the fluorescence was taken into account in order to yield an SV constant that is solely dependent on the singlet exciton diffusion length (l_D). The SV equation reads (Lakowicz 2011):

$$\frac{PLQY_0}{PLQY([Eu^{3+}])} = 1 + K_{SV}[Eu^{3+}], \tag{S1}$$

where $[Eu^{3+}]$ is the Eu^{3+} concentration and $PLQY_0$ is the unquenched PLQY of the ligand fluorescence, i.e. at $[Eu^{3+}] = 0$. In Figure S4 (A) the PLQY values of the ligand fluorescence are shown as a function of Eu^{3+} doping concentration. From those data, an SV plot was extracted and is shown in Figure S4 (B). A dimensionless SV constant (K_{SV}) of 3.9 ± 0.4 was determined by a linear fit, where the uncertainty is estimated based on the slope's standard deviation of the linear fit. Please note, that each data point was weighted by the inverse of its uncertainty (based on the measurement error) for the linear regression. However, using the ligand length s_l and assuming that in a volume of s_l^3 in average one Eu^{3+} atom is placed for the 100% Eu^{3+} doping case, the SV constant becomes $K_{SV} = (3.9 \pm 0.4)s_l^3$. Employing the Smoluchowski equation, this SV constant can be connected to a singlet exciton diffusion length:

$$l_D = \sqrt{\frac{6K_{SV}}{4\pi R}}, \tag{S2}$$

where R is the interaction radius and is chosen to be $s_l/2$, leading to:

$$l_D = (1.9 \pm 0.1)s_l. \tag{S3}$$

As a side note, this value can be seen as an upper bound since: i) the assumption that there is only one Eu^{3+} per ligand is likely an underestimation; and ii) R is given by the radius of the exciton plus the radius of the quenching species and therefore tends to be larger than $s_l/2$.
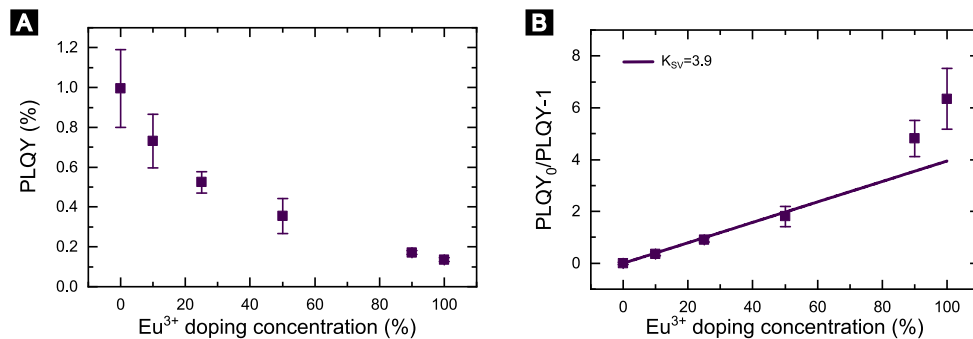
Figure S9: Plots for the Stern-Volmer analysis. (A) Photoluminescence quantum yield (PLQY) of the ligand fluorescence as a function of Eu^{3+} doping concentration in the Y-based coordination polymer. The stated values and error bars are determined from five measurements at different sample positions. (B) SV plot based on the PLQY values in (A) accompanied by a linear fit with a slope of 3.9 ± 0.4. The error bars are determined by propagating the errors from the PLQY values. Related to Figure 2.

Synthesis
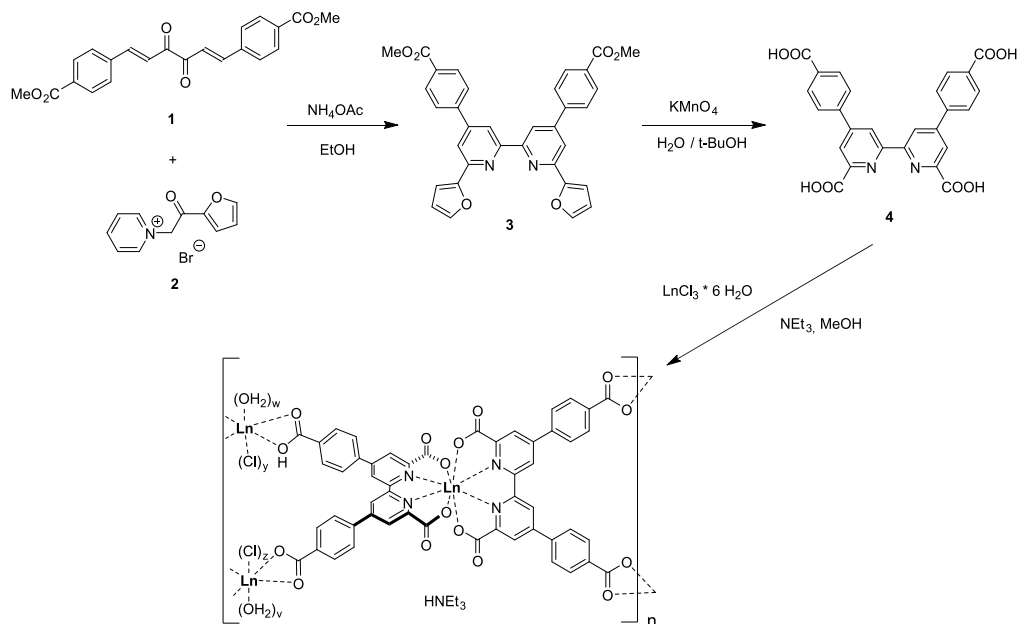
General

All commercially available chemicals for the synthetic and analytical work were purchased and used without any further purification steps. CDCl$_3$ and [D$_6$]-DMSO for NMR spectroscopy had 99.8 % deuteration level. NMR spectra were acquired on a Bruker instrument Avance II+400 (^{1}H: 400 MHz). Solid-state ^{1}H MAS NMR spectra were obtained on a Bruker AVII+500 (^{1}H: 500 MHz) standard bore spectrometer using a 2.5 mm MAS broadband probe head. Powdered samples were placed in a 2.5 mm (o.d.) zirconia rotor and MAS NMR spectra were obtained at spinning rates of 15 kHz. All chemical shifts (δ) for the NMR spectra are given in parts per million (ppm) and relative to the usual standard (tetramethylsilane, TMS). The chemical shift range was calibrated using the residual solvent signals as internal reference. Mass spectrometry was performed using a Bruker Daltonics Esquire 3000plus instrument (ESI mode). Elemental analyses were performed by the Analytical Facility of the Institute of Inorganic Chemistry (University of Tübingen) using a Vario MICRO EL analyzer.
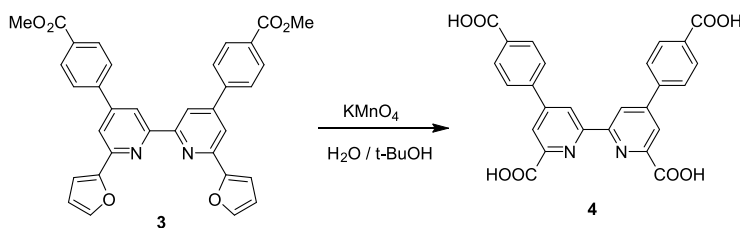
Bipyridine 3
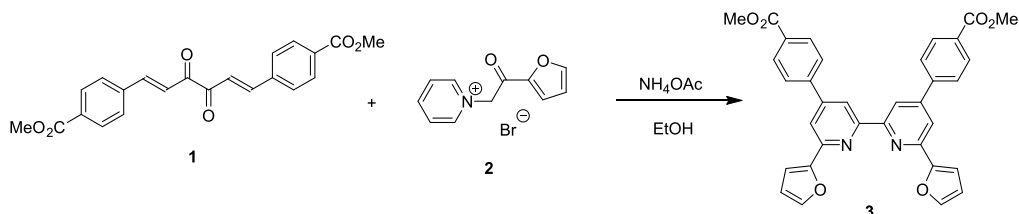
Diketone **1** (250 mg, 0.66 mmol, 1.0 equiv.) (Renouard and Grätzel 2001), pyridinium salt **2** (350 mg, 1.31 mmol, 2.0 equivs.) (Fujimori, Wirsching, and Janda 2003), and NH_4OAc (1.31 g, 17.03 mmol, 26 equivs.) were suspended in EtOH (25 mL) and refluxed for 21 h. The mixture was allowed to cool to room temperature. The precipitate was collected on a Büchner funnel, washed with EtOH, and dried under reduced pressure to give title compound **3** as a light beige solid (230 mg, 0.41 mmol, 63 %).

^{1}H NMR (400 MHz, CDCl$_3$): δ = 8.72 (d, J = 1.6 Hz, 2H), 8.23 (d, J = 8.3 Hz, 4H), 8.02 (d, J = 1.7 Hz, 2H), 7.93 (d, J = 8.3 Hz, 4H), 7.61 (br s, 2H), 7.35 (d, J = 3.4 Hz, 2H), 6.61 (dd, J = 3.3, 1.8 Hz, 2H), 3.99 (s, 6H) ppm. MS (ESI, pos. mode): m/z (%) = 557.0 (100, [M+H]+), 634.1 (46, [M+H+NH$_4$OAc]+). Anal. Calcd for $C_{34}H_{24}N_2O_6 \cdot 2.5\ H_2O$ (M$_r$ = 601.61): C, 67.88; H, 4.86; N, 4.66. Found: C, 67.38; H, 4.76; N, 5.03.

Tetracarboxylic acid ligand 4

A mixture of bipyridine **3** (1.00 g, 1.8 mmol, 1.0 equiv.), tert-butyl alcohol (200 mL) and water (40 mL) was heated to 80°C (bath temperature) and KMnO$_4$ (3.70 g, 23.4 mmol, 13 equivs.) was added in portions (in analogy to a reported procedure (D. D. Weller, Luellen, and D. L. Weller 1982)).

11

After stirring for 24 h, the suspension was filtered over celite on a Büchner funnel while hot to remove MnO_2 and the solid was washed with a mixture of tert-butyl alcohol / water (20 mL / 80 mL). Solvents in the filtrate were evaporated under reduced pressure until a minimum of water remained. The aqueous solution was acidified with 2 M HCl and the precipitate was collected on a Büchner funnel, washed with water, and dried in vacuo to give title compound **4** as a light beige solid (600 mg, 1.3 mol, 72 %).

^{1}H NMR (400 MHz, [D_6]-DMSO): $\delta = 9.11$ (br s, 2 H), 8.44 (br s, 2 H), 8.11 (br s, 8 H) ppm. MS (ESI, neg. mode): m/z (%) = 483.0 (100, [M-H]-). Anal. Calcd for $C_{26}H_{16}N_2O_8 \cdot 3.5\ H_2O$ (M_r = 547.48): C, 57.04; H, 4.23; N, 5.12. Found: C, 57.19; H, 3.71; N, 5.07.
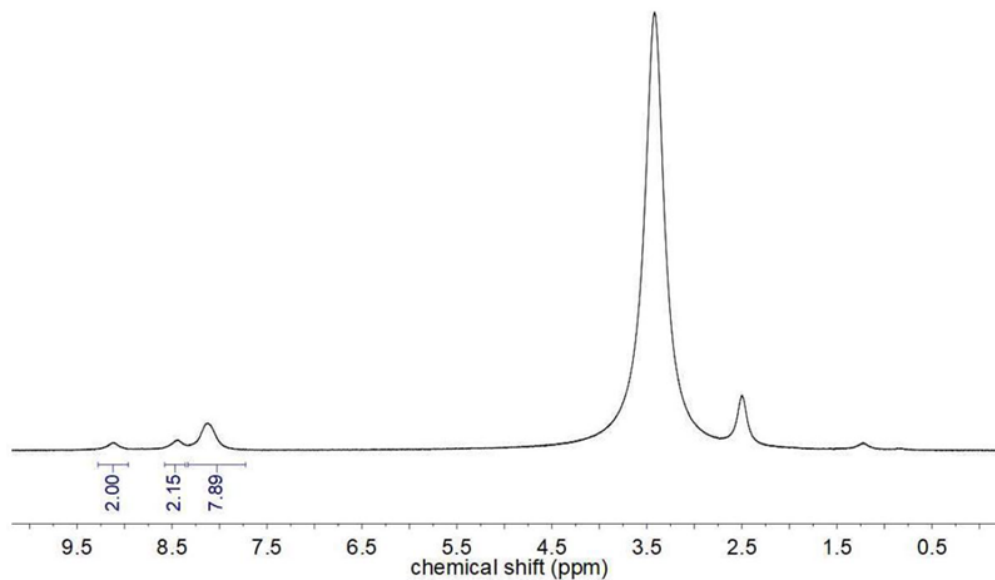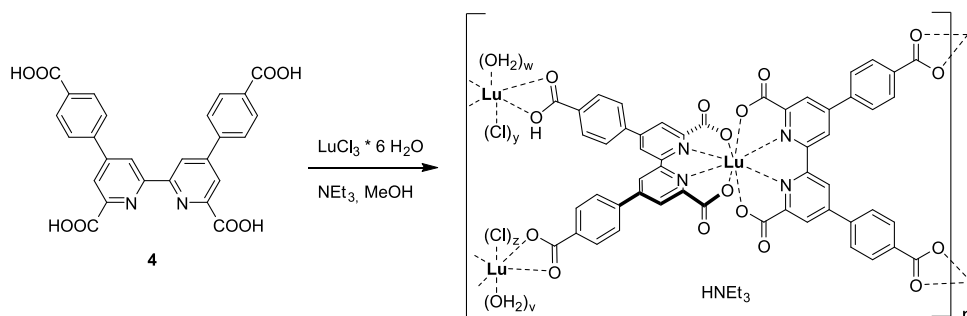

Figure S10: ^{1}H NMR (400 MHz, [D_6]-DMSO) of **4**. Related to Figure 1A.

Lutetium coordination polymer

Tetracarboxylic acid **4** (50 mg, 0.091 mmol, 1.0 equiv.) was suspended in dry MeOH (10 mL) and a solution of $LuCl_3 \cdot 6\ H_2O$ (38.9 mg, 0.10 mmol, 1.1 equiv.) in dry MeOH (2 mL) was added. After 10 minutes of stirring, NEt_3 (0.10 g, 0.14 mL, 1.0 mmol, 11 equivs.) was added and the mixture was stirred for 30 minutes at room temperature. The precipitate was filtered on a Büchner funnel with a membrane filter (Nylon, 0.4 μm pore size), washed with ice-cold MeOH, and dried in vacuo to give the compound as a insoluble, light orange solid (50.2 mg, 62%).

Anal. Calcd for $C_{52}H_{25}N_4O_{16}Lu_3Cl_3 \cdot$ HNEt3 $\cdot$ 4 H_2O (M_r =1767.30): C, 39.42; H, 2,79; N, 3.96. Found: C, 39.73; H, 3.04; N, 3.77.

The composition of the obtained material with respect to the presence of triethylammonium ($HNEt_3^+$) was investigated using solid-state ^{1}H MAS NMR spectra (Figure S11). For this purpose, the spectra of tetracarboxylic acid **4** and the lutetium coordination polymer were compared. The spectrum of **4** (Figure S11, left, black) is dominated by the broad aromatic signals around ca. 8 ppm and the signals of the carboxylic acids showing up at ca. 14 ppm. The lutetium coordination polymer (Figure S11, left, red) shows three broad peaks, corresponding to the aromatic protons of the ligands (ca. 7.5 ppm, very similar to free ligand **4**) and the two bands for the equivalent CH_2 (ca. 2.5 ppm) and CH_3 (ca. 0 ppm) moieties in $HNEt_3$. Lorentzian deconvolution of the spectrum (Figure S11, right) using three components and comparing the integrals of the aromatic band with the CH_3 band gives a ratio of ca. 2:1 for ligand **4**:$HNEt_3$ (as seen similarly in the elemental analysis above).
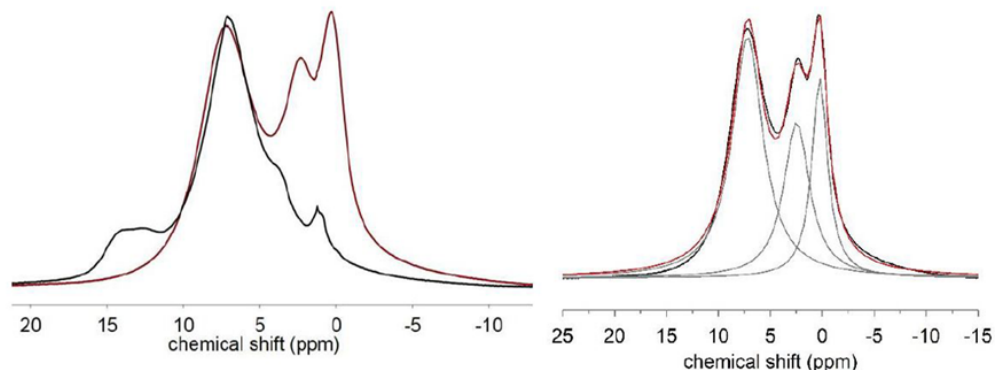
13

Figure S11: Solid-State ^{1}H MAS NMR spectra (500 MHz): Left – Spectra of **4** (black) and the lutetium coordination polymer (red); Right: Measured spectrum of the lutetium coordination polymer (black) with Lorentzian fit (3 individual Lorentzians in grey and cumulative fit function in red). Related to Figure 1A.

Yttrium coordination polymer

The yttrium compound was prepared in the same manner as for the lutetium compound starting from **4** (20 mg) and $YCl_3 \cdot 6\ H_2O$ (12.1 mg) yielding a light orange solid (20 mg, 73%).

Statistical Europium/Yttrium coordination polymer (50% Y / 50% Eu)

The Eu/Y compound was prepared in the same general manner as for the lutetium compound starting from **4** (20 mg) and a 50:50 mixture of $YCl_3 \cdot 6$ H_2O (6.1 mg) and $EuCl_3 \cdot 6\ H_2O$ (7.3 mg) yielding a light orange solid (23 mg, 79%).

References

Fujimori, T., Wirsching, P., and Janda, K. D. (2003). Preparation of a Kröhnke Pyridine Combinatorial Library Suitable for Solution-Phase Biological Screening. *J. Comb. Chem.* 5.5, 625–631.

Kruck, C., Nazari, P., Dee, C., Richards, B. S., Turshatov, A., and Seitz, M. (2019). Efficient Ytterbium Near-Infrared Luminophore Based on a Nondeuterated Ligand. *norg. Chem.* 58.10, 6959–6965.

Lakowicz, J. R. (2011). *Principles of Fluorescence Spectroscopy*. Springer.

Mello, J. C. de, Wittmann, H. F., and Friend, R. H. (1997). An improved experimental determination of external photoluminescence quantum efficiency. *Adv. Mater.* 9.3, 230–232.

Renouard, T. and Grätzel, M. (2001). Functionalized tetradentate ligands for Ru-sensitized solar cells. *Tetrahedron* 57.38, 8145–8150.

Weller, D. D., Luellen, G. R., and Weller, D. L. (1982). Synthesis of 4-arylpyridines. *J. Org. Chem* 47.24, 4803–4806.